Journal of Materials Chemistry C

Metal Surface Effects on Single Upconverting Nanoparticle Luminescence and Thermometry Signals

Journal:	*Journal of Materials Chemistry C*
Manuscript ID	TC-ART-09-2024-003911.R1
Article Type:	Paper
Date Submitted by the Author:	21-Oct-2024
Complete List of Authors:	Ye, Ziyang; University of Rochester Signor, Laura; University of Rochester Cohan, Molly; University of Rochester; The College of Wooster, Department of Physics Pickel, Andrea; University of Rochester

Metal Surface Effects on Single Upconverting Nanoparticle Luminescence and Thermometry Signals

Ziyang Ye[a], Laura Signor[b], Molly Cohan[b,c], and Andrea D. Pickel[a,b,d,*]

[a] Materials Science Program, University of Rochester, Rochester, NY 14627

[b] The Institute of Optics, University of Rochester, Rochester, NY 14627

[c] Department of Physics, The College of Wooster, Wooster, OH 44691

[d] Department of Mechanical Engineering, University of Rochester, Rochester, NY 14627

*Corresponding author. Email: apickel@ur.rochester.edu

Metal surfaces can alter the luminescence emitted by nanoparticles through a variety of effects including quenching, plasmonic enhancement, and optical interference-, reflection-, and absorption-related phenomena. While many of these effects are well-established, multiple such effects typically occur in parallel in realistic measurement scenarios, making the relative importance of each effect difficult to discern. As imaging and sensing applications in which luminescent nanoparticles are placed on metal surfaces continue to grow, a detailed understanding of how metal surfaces modify nanoparticle luminescence is increasingly important for optimizing and ensuring correct interpretation of the measurement results. Here, we systematically investigate how metal surfaces affect the luminescence emitted by individual $NaYF_4$:Yb^{3+},Er^{3+} upconverting nanoparticles (UCNPs) ~27 nm in diameter using a judiciously selected set of five different metal coatings with varying optical and thermal properties. We find that the average single-UCNP emission intensity is determined by an interplay between quenching and reflection effects. Consequently, the average single-UCNP emission intensity is correlated with the reflectance of the underlying metal coating, but non-radiative decay rate changes also play an important role, leading to different average single-UCNP emission intensities for metal coatings with near-identical reflectances. We also evaluate metal surface effects on the common ratiometric thermometry signal of $NaYF_4$:Yb^{3+},Er^{3+} UCNPs and find that the intrinsic temperature dependence of the luminescence intensity ratio is unaffected by the underlying material. The only differences observed are the result of laser-induced heating for sufficiently absorbing metal coatings on low thermal conductivity substrates, in accordance with the predictions of an analytical heat transfer model.

1. Introduction

The ability of nearby metal surfaces to modify the emission from luminescent materials has been established for many decades. After Purcell[1] proposed that placing an emitter in a cavity could change its spontaneous emission rate, Drexhage et al.[2] reported seminal experiments in which metal surfaces maintained at different fixed distances from luminescent Eu^{3+}-containing complexes were shown to modify their luminescence decay times, establishing how controlling the local density of states of an emitter can in turn alter its luminescence characteristics. More recently, plasmonic nanostructures, which are often composed of noble metals, have been used extensively to increase luminescence intensity by enhancing both absorption and emission processes[3,4]. Metal surfaces and metallic nanoparticles are also known to quench luminescence through the creation of new non-radiative decay pathways[5,6], leading to competition between quenching effects and enhancement mechanisms[7]. Additionally, when the light source used to excite luminescent emitters is reflected by a metal surface, constructive or destructive interference that affects the excitation intensity seen by the emitter[8,9], along with the additional chance to absorb reflected photons, can alter the luminescence intensity. Similarly, luminescent emission reflected by a metal surface can augment the detected intensity[10,11]. Furthermore, if radiation absorbed by a metal surface induces a local temperature rise, changes in the luminescence can also be observed as a result of its temperature dependence[12]. Because of these various competing effects, even the basic question of whether placing an emitter on or near a metal surface will increase or decrease its luminescence intensity can be challenging to answer.

Upconverting nanoparticles (UCNPs) are lanthanide-doped inorganic probes with wide-ranging applications including biological imaging[13] and sensing of quantities such as pH, pressure, force, electric field, and temperature[14]. Plasmon-enhanced upconversion is a well-established strategy for increasing UCNP emission intensity[15,16], often involving noble metal nanostructures, and the concurrent presence of metal quenching effects has been identified in this context[11]. As thermometry applications that require placing UCNPs on the metal surfaces of electronic devices or photonic structures continue to grow[17], interference effects that originate from metal surfaces and can distort the temperature-dependent UCNP luminescence have also been reported. Van Swieten et al.[18] showed how a few-μm-thick layer of UCNPs placed on a molybdenum spiral heater could produce erroneous temperature readings due to spectral distortions resulting from the heater surface acting as a mirror. Vonk et al.[19] later performed experiments in which UCNP monolayers were placed at controlled distances from a gold mirror, further demonstrating that the same artifact can lead to equivalent temperature errors as large as 250 K. These studies provide clear evidence of how complicated interactions between UCNPs and metal surfaces can directly impact their imaging and sensing applications, yet other aspects of UCNP-metal surface interactions remain largely unexplored, underscoring the need for continued investigation. Isolating the influence of different contributing factors is important for both maximizing the luminescence signal and verifying that changes observed in the luminescence are attributed to the correct underlying physical phenomena.

Here, we consider isolated individual $NaYF_4$:Yb^{3+},Er^{3+} UCNPs, the most popular composition, placed directly on the surfaces of metal-coated substrates. In contrast with samples that involve a thicker layer of UCNPs or a dielectric spacer layer between the metal surface and UCNPs, this configuration avoids interference between the directly emitted and reflected UCNP

luminescence or reabsorption of the emitted luminescence[20]. Similarly, these planar metal films do not support localized surface plasmon resonances, allowing us to focus on how the intrinsic metal coating properties affect the UCNP emission. This scenario is also relevant to applications where UCNPs are placed directly on metal surfaces, such as thermometry applications where direct contact is desirable to minimize thermal resistance between the UCNPs and sample surfaces. We selected five metal coatings with a range of optical and thermal properties that were deposited on substrates with varying thermal conductivities, since the thermal conductivity of the underlying substrate in part determines the temperature rise resulting from any laser heating. Carefully characterizing the average single-UCNP emission intensity by imaging > 80 single particles per sample allows us to determine how each metal affects the emission intensity, while luminescence lifetime measurements elucidate the role of reflection effects vs. quenching resulting from increased non-radiative decay. After calibrating the temperature-dependent luminescence intensity ratio for single UCNPs on multiple substrates, we measured the ratiometric thermometry signal as a function of the excitation laser intensity for single UCNPs on 12 samples to assess the impact of different metal coatings on the temperature-dependent UCNP emission. The results of this study provide fundamental insights into UCNP-metal surface interactions and can inform diverse imaging and sensing applications of UCNPs.

2. Experimental Section

2.1 Metal Coating Selection and Deposition

Metal coatings approximately 50 nm in thickness (ESI Fig. S1) were deposited onto borosilicate glass and sapphire substrates by electron beam evaporation. Prior to deposition, the substrates were cleaned by sonication for ten minutes each in acetone, isopropyl alcohol, and deionized water, followed by 30 s of plasma cleaning. The metal coatings were deposited to cover half of the substrate, such that measurements of UCNPs on a single sample could be performed on both uncoated or metal-coated borosilicate glass or sapphire. The five metals selected were gold (Au), silver (Ag), nickel (Ni), chromium (Cr), and titanium (Ti). These different metals provide a range of optical reflectance (R) values at our excitation laser wavelength of 976 nm. We experimentally characterized R and the transmittance (T) of all five metal films on borosilicate glass substrates using a PerkinElmer Lambda 900 UV/VIS/NIR spectrometer (ESI Fig. S2 and Table S1). Au and Ag are highly reflective at 976 nm, both with R of 0.99. Ni has a R value of 0.83, while Cr and Ti are both less reflective, with R values of 0.71 and 0.62, respectively. The absorptance (A) values of the metal coatings can be calculated as $A = 1 - R - T$. The Au, Ag, and Ni coatings all have $T < 0.02$, while the Cr and Ti coatings display non-negligible T. The thermal conductivities (k) of these metals likewise vary, with typical bulk values of approximately 430 W m^{-1} K^{-1} for Ag, 320 W m^{-1} K^{-1} for Au, 90 W m^{-1} K^{-1} for Ni, 70 – 90 W m^{-1} K^{-1} for Cr, and 20 W m^{-1} K^{-1} for Ti[21]. Thin film k values are expected to be reduced below the corresponding bulk values due to surface and grain boundary scattering, and experimental measurements for these metals report thin film k values reduced by half or more of their corresponding bulk values[22-26]. Borosilicate glass and sapphire are both highly transparent to our 976 nm excitation laser, while their contrasting thermal conductivities (~1 W m^{-1} K^{-1} for borosilicate glass and ~30 – 40 W m^{-1} K^{-1} for sapphire) provide control over the temperature rise resulting from laser heating.

2.2 UCNP Characterization and Deposition

$NaYF_4$ UCNPs doped with 20 at.% Yb^{3+} and 2 at.% Er^{3+} dispersed in cyclohexane were purchased from CD Bioparticles. To prepare the UCNPs for transmission electron microscopy (TEM) characterization, the UCNP solution was diluted tenfold from its as-received concentration of 20 mg/mL to a final concentration of 2 mg/mL and then drop cast onto a TEM grid with a lacey carbon support film. From analysis of TEM images shown in ESI Fig. S3, we confirm the hexagonal prism morphology of the UCNPs and determine an average UCNP diameter of ~27 nm and a similar average height of ~26 nm (ESI Fig. S4). To prepare samples for optical measurements, the UCNP solution was diluted to a concentration of 0.03 mg/mL. Approximately 40 μL of solution was then spin coated onto each sample, which resulted in samples primarily consisting of isolated individual UCNPs spaced sufficiently far apart from one another such that their diffraction limited emission spots did not overlap. Scanning electron microscope (SEM) images of the UCNPs deposited on the metal coatings are shown in ESI Fig. S5.

2.3 Optical Imaging, Spectroscopy, and Lifetime Measurements

All optical measurements were performed using a custom-built confocal microscopy and spectroscopy system. A continuous wave 976 nm fiber-coupled diode laser (BL976-PAG500, Thorlabs) whose output was sent through a clean-up bandpass filter (LD01-975/10-25, Semrock) served as the excitation source. The laser beam was focused onto the sample surface using a 100x dry air objective lens with a numerical aperture of 0.8 (Nikon). A 775 nm shortpass dichroic mirror (zt775sp-2p-uf3, Chroma) both reflected the laser beam towards the sample and transmitted the upconverted luminescence. A piezo-controlled nanopositioning stage (Mad City Labs Nano-T115) was used to scan the samples and a thermal stage (custom version of HCS321Gi, Instec) was used for temperature calibration measurements. After passing through a shortpass filter (BSP01-785R-25, Semrock) to eliminate any residual excitation light, the emitted luminescence was directed through a 100 μm confocal pinhole and a bandpass filter (FF01-520/70-25, Semrock) and focused onto an avalanche photodiode (APD; Micro Photon Devices PDM Series) for single-UCNP imaging and lifetime measurements. For single-UCNP spectroscopy, the luminescence was instead directed to a spectrometer (Andor Kymera 193i spectrograph with an iDus 420 CCD camera). To obtain single-UCNP lifetime decay curves, the 976 nm excitation laser output was modulated using a function generator and photon arrival times relative to the modulated laser output were tagged using a time-correlated single-photon counting module (PicoHarp 300, PicoQuant).

3. Results and Discussion

3.1 Metal surface effects on single-UCNP emission intensities

To characterize the average single-UCNP emission intensity for UCNPs on different surfaces, we imaged > 100 distinct emission spots (including > 80 single particles) per substrate using our APD. We then constructed histograms of this data, an established approach for identifying the characteristic emission intensity of a single UCNP[27]. Imaging many individual UCNPs on each substrate also allows us to more clearly separate metal surface effects from particle-to-particle variability. Fig. 1a shows the histogram for UCNPs on an uncoated sapphire substrate. By fitting a Gaussian to the first peak of the histogram, which corresponds to single UCNPs, we can extract a characteristic single-UCNP emission intensity of approximately 480

counts per second (cnt/s). We can then compare analogous values for UCNPs imaged on metal-coated sapphire to this baseline value to evaluate the influence of different metal coatings on the UCNP emission intensity. These measurements were performed using sapphire substrates since the higher thermal conductivity of sapphire relative to glass helps mitigate potential laser heating. To evaluate potential laser heating, we calculated the steady-state temperature rise resulting from continuous wave laser irradiation using analytical solutions for heat conduction in a layered system incorporating radial effects[28,29] (ESI Note S1). Since direct characterization of the metal coating k values was not available, we considered a range of possible k based on reported thin film values. Our calculations indicate the thermal conductivity of sapphire is sufficiently high to avoid laser heating large enough to result in appreciable thermal quenching (estimated to be ≤ 16 K for all five metals coatings for the range of k considered) at the excitation intensity of 2.37 x 10^5 W cm^{-2} used in these experiments. Experimental measurements presented later in Section 3.4 of the manuscript also show no detectable laser heating for excitation intensities up to 6.32 x 10^5 W cm^{-2} within our measurement uncertainty of approximately ± 10 K.

For substrates coated with Ti, Cr, and Ni, the characteristic single-UCNP emission intensity is reduced from the baseline value of 480 cnt/s to approximately 370 cnt/s, 380 cnt/s, and 400 cnt/s, respectively, as shown in Fig. 1b-d. This reduction in counts is indicative of a metal quenching effect. For an Ag-coated substrate, the single-UCNP emission intensity of approximately 470 counts/s is comparable to the baseline value (Fig. 1e), while for an Au-coated substrate, the single-UCNP emission intensity increases to approximately 610 cnt/s (Fig. 1f). Fig. 1g plots the single-UCNP emission intensity vs. the measured R values for each metal coating. The single-UCNP intensity is correlated with R of the underlying metal, indicating that reflection-related effects, such as additional opportunities for UCNPs to absorb reflected excitation light and reflection of back-emitted luminescence towards the detector, impact the recorded single-UCNP emission intensity. These results suggest that for coatings with sufficiently high R, reflection-related enhancement can compensate for or even overcome metal quenching effects. Simultaneously, it is evident that R alone does not determine the detected emission intensity, which can be observed most clearly in the case of Au vs. Ag. Both coatings have the same measured R value of 0.99, yet the single-UCNP intensity for Au-coated sapphire is ~30% higher than that for Ag-coated sapphire, implying that material-dependent quenching or enhancement effects are also an important contributing factor.

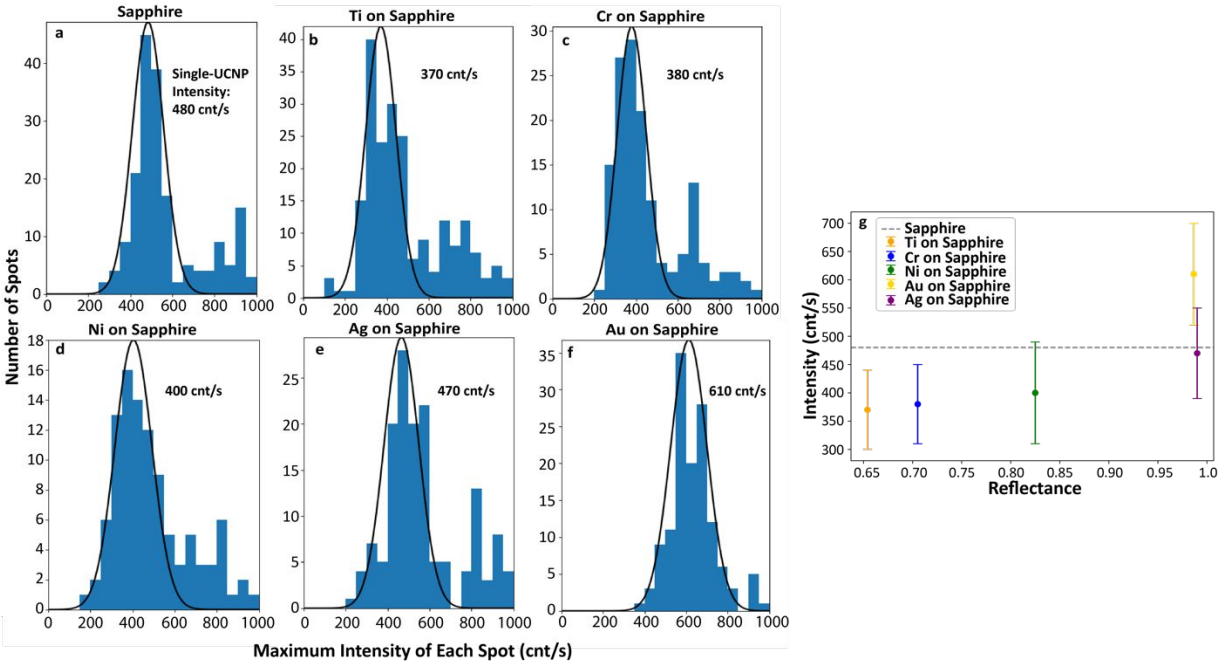

Fig. 1 Histograms of the maximum number of counts per second (cnt/s) for emission spots originating from samples primarily consisting of single UCNPs on various substrates. The first peak of each histogram was fit with a Gaussian distribution to find the characteristic emission intensity for single UCNPs on (a) an uncoated sapphire substrate (480 cnt/s) and sapphire substrates coated with (b) Ti (370 cnt/s), (c) Cr (380 cnt/s), (d) Ni (400 cnt/s), (e) Ag (470 cnt/s), and (f) Au (610 cnt/s). (g) Characteristic single-UCNP emission intensities determined from (b)-(f) plotted as a function of *R* of the underlying metal coating. Error bars represent the standard deviations of the fitted Gaussians. The 976 nm laser excitation intensity used for these measurements was 2.37 x 10^5 W cm^{-2}.

Others have compared the emission intensity from UCNPs on uncoated and metal-coated substrates, largely in the context of recording emission from UCNPs on a flat metal film composed of the same material as a plasmonic nanostructure to better isolate the plasmonic nanostructure's enhancement capabilities. These previous reports diverge in their findings of whether a metal-coated substrate augments or diminishes UCNP emission intensity relative to an uncoated substrate. For example, Sun et al.[30] reported 14-fold quenching of the green emission from $NaYF_4$:Yb^{3+},Er^{3+} UCNPs on a flat Au-coated surface relative to uncoated glass. Conversely, Wiesholler et al.[31] found that the emission intensity from $NaYF_4$:Yb^{3+},Tm^{3+} UCNPs on Au-coated glass was enhanced compared to uncoated glass, albeit not as strongly as for an Au plasmonic nanostructure, which was attributed to propagating surface plasmon effects. Xu et al.[32] also compared the green emission from $NaYF_4$:Yb^{3+},Er^{3+} UCNPs on Au-coated and uncoated glass and observed that the emission intensity from UCNPs on Au-coated glass could exceed that from UCNPs on uncoated glass at higher excitation intensities of ~10^4 W cm^{-2}. These latter two studies align with our results for an Au coating, with the work of Xu et al. pointing to excitation intensity as one factor that can influence how a given metal impacts UCNP emission intensity. Our work focuses on single UCNPs, which inherently require high excitation intensities, typically ~10^4 – 10^6 W cm^{-2}. While previous studies have focused on a single metal, here we directly compare the

effects of different metals with varying optical and thermal properties under otherwise identical conditions and using UCNPs from the same batch, potentially mitigating other confounding factors.

3.2 Single-UCNP lifetime measurements on uncoated and metal-coated substrates

To further explore the hypothesis that material-dependent metal quenching effects could explain differences in the average single-UCNP emission intensity for metal coatings with similar *R* values, we recorded lifetime decay data for individual UCNPs on different substrates and fit the results to an exponential decay (Fig. 2a). The bandpass filter used for these measurements has a transmission band of 485 – 555 nm and we thus measure the combined lifetime of the $^2H_{11/2}$ and $^4S_{3/2}$ excited states[33,34]. For single UCNPs on an uncoated sapphire substrate, we obtain an average lifetime (τ) of 125 μs. For single UCNPs on metal-coated substrates, the τ values are all lower compared to this baseline, as expected for increased non-radiative decay caused by the metal coatings[11], but the amount by which the average τ is reduced varies among the different metals (Fig. 2b). Considering Au and Ag, we indeed observe a larger reduction in the average τ for single UCNPs on Ag than Au (47 μs for Ag vs. 67 μs for Au), indicative of a stronger increase in non-radiative decay on Ag. For the other three metals, we observe that Ni results in the smallest reduction in the average τ (60 μs, comparable to Au), while Cr and Ti lead to lower average τ values of 47 μs and 27 μs, respectively.

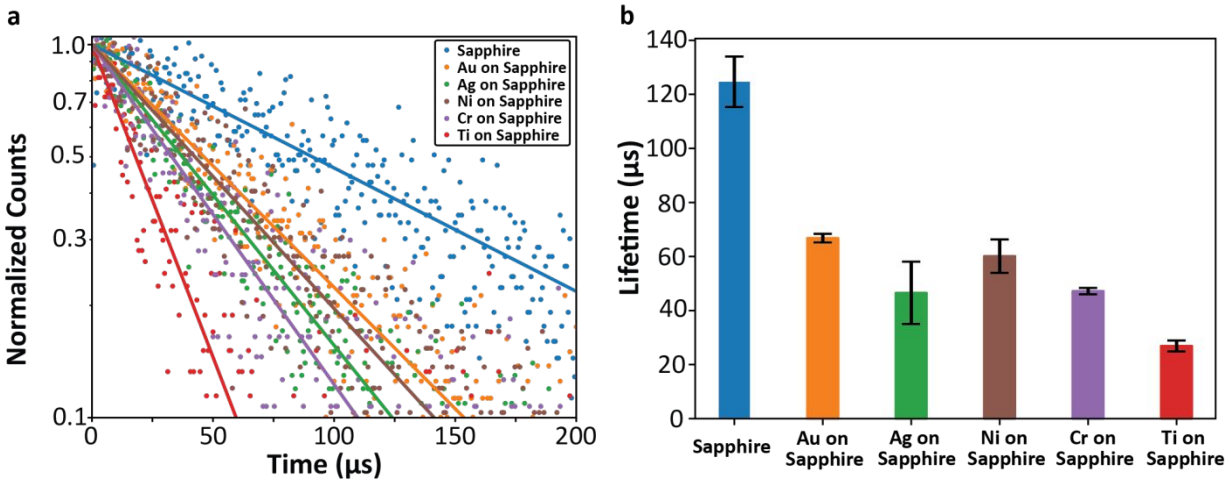

Fig. 2 (a) Representative lifetime decay curves for individual UCNPs on uncoated sapphire and sapphire substrates coated with Au, Ag, Ni, Cr, and Ti, fit with single exponential decays and normalized. The excitation intensity and integration time were 1.58 x 10^5 W cm^{-2} and 180 s, respectively. The excitation modulation for all measurements was a 1.5 kHz square wave. (b) Mean luminescence lifetimes (τ) for single UCNPs on uncoated sapphire and metal-coated sapphire substrates determined from single exponential fits to two consecutive measurements. Error bars represent the standard deviation.

Although the differences in the average single-UCNP emission intensities for Ni, Cr, and Ti are not as pronounced as for Au and Ag, we note that the emission intensities on these three lower *R* metal coatings follow the same trend with τ, with the highest emission intensity

corresponding to the largest τ and vice versa. Simultaneously, the results summarized in Fig. 2b clearly demonstrate that differences in τ alone cannot explain the variation in UCNP emission intensity shown in Fig. 1: despite UCNPs on Ag and Cr having similar τ values of ~47 μs, along with UCNPs on Au and Ni having similar τ values of ~60 – 70 μs, the emission intensity of UCNPs on Cr and Ni is markedly lower than that of UCNPs on Ag and Au. This finding further supports the assertion that *R* is critical in determining the emission intensity. Taken together, the results in Fig. 1 and Fig. 2 suggest that the average emission intensity for single UCNPs on metal surfaces is governed by an interplay between quenching and reflection effects, where *R* of the underlying metal plays a major role in determining how the emission intensity compares to the baseline value for an uncoated substrate, while differences in non-radiative decay deduced from the measured τ values can account, at least in part, for the emission intensity variation observed for metals with similar *R*. While a detailed investigation of possible material-specific enhancement effects is beyond the scope of this study, we also note that such effects potentially also exist and could contribute to the observed differences between Au and Ag, for example.

3.3 Single-UCNP ratiometric thermometry calibrations on uncoated and metal-coated substrates

After demonstrating how various metal coatings can have different impacts on single-UCNP emission intensities, we next evaluated whether these same coatings could alter the relative intensities of spectral features that frequently facilitate ratiometric thermometry[35,36]. After multiple Yb^{3+} ions absorb incident 976 nm radiation and transfer this energy sequentially to a single Er^{3+} ion, the Er^{3+} decays non-radiatively from its $^4F_{7/2}$ excited state to its $^2H_{11/2}$ and $^4S_{3/2}$ manifolds. Radiative relaxation back to the ground state subsequently yields emission in the green wavelength range. Due to the small energy gap between $^2H_{11/2}$ and $^4S_{3/2}$, the relative emission intensity originating from these manifolds can be described by the following Arrhenius-type relationship[37],

$$\frac{\int_{\lambda_1}^{\lambda_2} I(\lambda)d\lambda}{\int_{\lambda_2}^{\lambda_3} I(\lambda)d\lambda} \equiv r = Aexp\Big(-\frac{\Delta E}{k_B T}\Big), \quad (1)$$

where r is the temperature (T)-dependent luminescence intensity ratio, $I(\lambda)$ is the emission spectrum, ΔE is the energy difference between $^2H_{11/2}$ and $^4S_{3/2}$, k_B is the Boltzmann constant, and A is a constant related to the radiative transition rates from $^2H_{11/2}$ and $^4S_{3/2}$ to $^4I_{15/2}$. Fig. 3a shows normalized emission spectra for individual $NaYF_4$:Yb^{3+},Er^{3+} UCNPs at room temperature on various substrates between 513 nm – 550 nm, with the wavelength bounds λ_1, λ_2, and λ_3 that we use here labeled accordingly. If metal coatings were found to impact the UCNP emission intensity in a spectrally non-uniform manner, such effects could alter the ratiometric thermometry signal. However, as observed in Fig. 3a, the normalized room temperature emission spectra all agree well with one another, indicating that the metal coating-induced emission changes are spectrally uniform over this wavelength range. The subset of substrates selected for these measurements, which are uncoated borosilicate glass and sapphire, Au-coated borosilicate glass, and Ti-coated sapphire, were selected to encompass a broad range of optical and thermal properties and to assess metal coatings that enhance and reduce UCNP emission relative to uncoated substrates based on the results from Fig. 1. Fig. 3b shows r vs. T calibration curves measured using our thermal stage for individual UCNPs on the same set of substrates as in Fig. 3a. The calibration curves recorded for UCNPs on different substrates are again in good agreement, confirming that the metal coating

effects remain spectrally uniform at elevated temperatures. The temperature sensitivity of the UCNPs is consistent across different substrates and is comparable to reported values for other single $NaYF_4$:Yb^{3+},Er^{3+} UCNPs and UCNP ensembles (ESI Fig. S6).

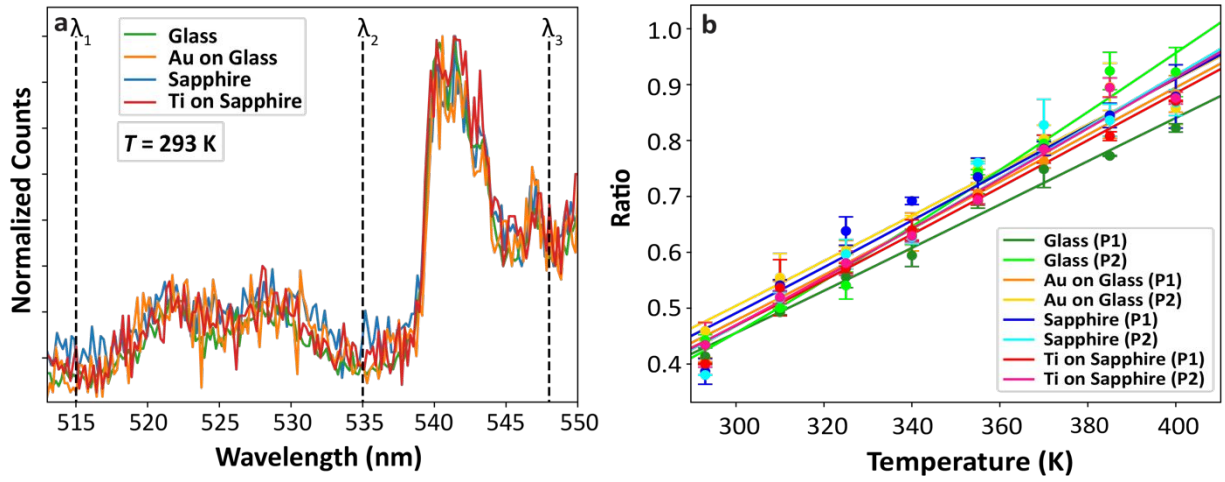

Fig. 3 Single-UCNP luminescence intensity ratio (r) vs. temperature (T) calibrations on four different substrates: uncoated borosilicate glass, Au-coated borosilicate glass, uncoated sapphire, and Ti-coated sapphire. The excitation intensity of 1.58 x 10^5 W cm^{-2} was selected to minimize the potential for laser heating. (a) Normalized luminescence spectra at room temperature (293 K) for single UCNPs on these four different substrates. The integration bounds used to calculate r are represented by the black dashed lines at wavelengths λ_1, λ_2, and λ_3. The integration time for all spectra was 120 s. (b) r vs. T calibrations for two particles, P1 and P2, on each different substrate. Error bars represent the standard deviation calculated from two consecutive measurements. The solid lines are fits to Eq. 1 for each particle.

3.4 Excitation intensity effects on the ratiometric thermometry signal for single UCNPs on uncoated and metal-coated substrates

Having established that the intrinsic $r(T)$ dependence is unaffected by the metal coatings, we investigated how r changes as a function of the laser excitation intensity (I_{exc}) for uncoated and metal-coated substrates. While the $r(T)$ calibrations shown in Fig. 3b confirm that metal coatings affect the UCNP emission intensity uniformly over the relevant wavelength range for ratiometric thermometry at I_{exc} = 1.58 x 10^5 W cm^{-2}, it was unknown if this behavior would hold true at higher I_{exc}. Furthermore, for samples with a combination of sufficiently high A and low k, we also expect to observe differences in the $r(I_{exc})$ behavior due to laser heating of the substrate. We first considered uncoated borosilicate glass and sapphire and both borosilicate glass and sapphire coated with Au and Ag. As noted previously, uncoated borosilicate glass and sapphire are highly transparent to our 976 nm excitation laser and thus no measurable temperature rise should be observed. Ag and Au have sufficiently low A and high k relative to the other metals such that we estimate the temperature rise will be no more than a few degrees at the maximum I_{exc} used in our measurements, even considering possible metal coating k values reduced by half of their corresponding bulk values.

Fig. 4a shows measured r values as a function of I_{exc} for uncoated borosilicate glass and sapphire and Au- and Ag-coated borosilicate glass and sapphire. We observe that r initially increases before plateauing at higher values of I_{exc}. The initial increase in r is consistent with the apparent self-heating effect previously reported for $NaYF_4$:Yb^{3+},Er^{3+} UCNPs[34]. In brief, a combination of radiative and non-radiative relaxation from high energy Er^{3+} states that are populated at high I_{exc} increases r, even though the true UCNP temperature does not increase. Here, by extending our measurements to higher I_{exc} than prior work, we also observe a saturation in the increase of r with I_{exc} at the highest I_{exc} values. Importantly, the $r(I_{exc})$ behavior is essentially identical for all samples, further confirming that the increase in r is non-thermal: because these samples have different thermal properties, which in turn alters their heat dissipation capabilities, the magnitude of any laser-induced temperature rise should vary among samples. Consequently, if the increase in r were indicative of true heating, the magnitude of this increase would likewise vary. The invariance of the apparent self-heating effect among the subset of samples evaluated in Fig. 4a agrees with prior measurements demonstrating consistent $r(I_{exc})$ behavior for $NaYF_4$:Yb^{3+},Er^{3+} UCNPs on uncoated borosilicate glass and diamond and platinum-coated diamond[29]. The results further demonstrate that this non-thermal behavior generalizes across additional metal coatings.

Fig. 4b shows $r(I_{exc})$ measurements for Ni-, Cr- and Ti-coated sapphire and all five metal coatings on borosilicate glass. Again, uncoated borosilicate glass is highly transparent at 976 nm, so no measurable temperature rise should be observed. Fig. 4b also includes a shaded band representing the $r(I_{exc})$ increase originating solely from the apparent self-heating effect, which is obtained by taking the mean and standard deviation of all measurements from Fig. 4a and performing polynomial fits one standard deviation above and below the mean (ESI Fig. S7, Note S2, and Table S2). The $r(I_{exc})$ measurements for single UCNPs on Ni-, Cr- and Ti-coated sapphire fall into a similar range as the data from Fig. 4a, indicating that the $r(I_{exc})$ increase observed for these samples is predominantly driven by the non-thermal apparent self-heating effect. However, because our calculations indicate the potential for non-negligible laser heating of these sample for the range of possible *k* values we consider, we cannot eliminate the possibility that these samples experience laser heating that is undetectable within our measurement uncertainty of approximately ± 10 K.

Conversely, for single UCNPs on Ni-, Cr-, and Ti-coated borosilicate glass, we observe increases in r with I_{exc} that clearly exceed the increase expected from the non-thermal apparent self-heating effect alone. These measurements combine the $r(I_{exc})$ increase due to the apparent self-heating effect with an additional $r(I_{exc})$ increase caused by true laser heating, the latter of which results from the higher *A* and lower *k* of these metals relative to Au and Ag and the lower *k* of borosilicate glass relative to sapphire. Furthermore, the magnitude of the $r(I_{exc})$ increase scales as expected based on the *k* of each metal coating, given that *A* is very similar for these three coatings. Ti, which has the lowest *k*, displays the greatest increase in r, while Ni, which has the highest *k*, displays the smallest increase in r. To convert these increases in r with I_{exc} to temperature rises, we first subtract the apparent self-heating contribution, accounting for uncertainty in the non-thermal $r(I_{exc})$ behavior for each UCNP (since this contribution inherently cannot be isolated for UCNPs on substrates that experience laser heating) by considering the range of values represented by the shaded band in Fig. 4b (ESI Note S3). We then convert the remaining increase in r with I_{exc} to a temperature rise using the calibration curves shown in Fig. 3b (ESI

Note S3 and Table S3). Fig. 4c shows experimentally determined temperature rise values as a function of I_{exc} for Ni-, Cr-, and Ti-coated borosilicate glass, along with corresponding linear fits since the temperature rise will increase linearly with the absorbed laser power. Prior work has shown that single UCNPs with a 50 nm diameter capture the peak temperature in a laser-heated spot to an excellent approximation (within 0.01% error)[29] and the same will hold true for the ~27 nm diameter UCNPs employed here, since the smaller diameter only further reduces spatial averaging of the true temperature profile. We calculated the steady state temperature rise for each metal coating on borosilicate glass in Fig. 4c, again considering a range of possible k based on reported literature values, and we find that the experimentally measured temperature rises are consistent with this range (ESI Fig. S8, Table S4, and Note S4).

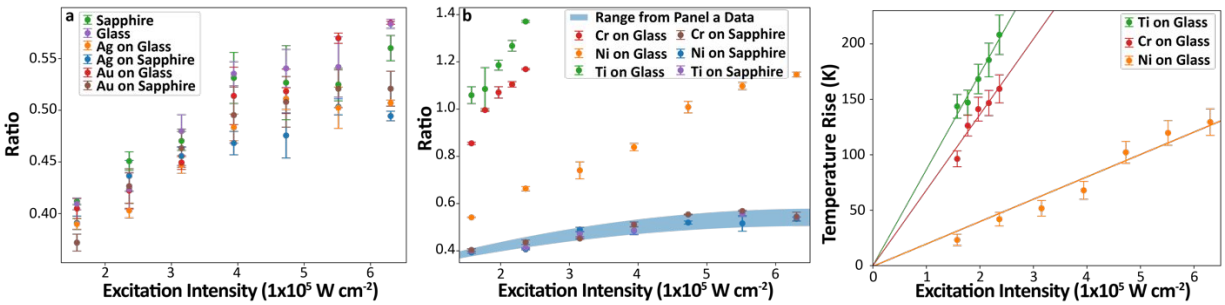

Fig. 4 (a) Luminescence intensity ratio (r) as a function of excitation intensity (I_{exc}) for single UCNPs on uncoated borosilicate glass and sapphire and Au- and Ag-coated borosilicate glass and sapphire. Error bars represent the standard deviation calculated from two consecutive measurements. Despite the different thermal properties of these substrates, r consistently increases with I_{exc} and then plateaus, indicating that this $r(I_{exc})$ increase is solely due to the non-thermal apparent self-heating effect. (b) The same measurements as in (a) for Ni-, Cr-, and Ti-coated borosilicate glass and sapphire. The blue shaded region represents the $r(I_{exc})$ increase solely from the apparent self-heating effect, which is obtained from polynomial fits to the data in (a) (ESI Note S2). The data for Ni-, Cr-, and Ti-coated sapphire fall into a similar range as that represented by the blue shaded band, indicating either negligible or undetectable laser heating. Meanwhile, single UCNPs on Ni-, Cr-, and Ti-coated borosilicate glass display a much larger $r(I_{exc})$ increase, resulting from a combination of the apparent self-heating effect and true laser heating. (c) Temperature rises determined from the measured r values in (b) after subtracting the non-thermal apparent self-heating contribution, along with corresponding linear fits. Error bars account for uncertainty originating from both the apparent-self heating effect and the use of a batch temperature calibration (ESI Note S3). For single UCNPs on Cr- and Ti-coated borosilicate glass, measurements were truncated at lower I_{exc} relative to Ni-coated borosilicate glass (denoted by the black dashed line) since the luminescent signal was lost at higher I_{exc}, likely due to UCNP thermal damage known to occur several hundred degrees above room temperature.

4. Conclusions

We explored the effects of different metal coatings on the luminescence intensities, lifetimes, and ratiometric thermometry signals of individual ~27 nm diameter $NaYF_4$:Yb^{3+},Er^{3+} UCNPs. We find that the average single-UCNP emission intensity is correlated with the

reflectance R of the underlying metal surface, with higher R metals augmenting the detected intensity, but material-specific metal quenching effects can lead to different intensities for metal coatings with near-identical R. These results provide heuristics for determining how the optical properties of different metals will affect single-UCNP emission intensities, while simultaneously underscoring the potential for complicated interactions with other metal surface effects. We further investigated the influence of metal coatings on the commonly applied ratiometric thermometry signal for single UCNPs, finding that the temperature-dependent behavior is consistent across uncoated and metal-coated substrates. As the laser excitation intensity I_{exc} is increased, we observe a non-thermal increase in the temperature-dependent ratio r in agreement with prior reports, which we further show is uniform across different metal coatings. For substrates with sufficiently high optical absorption and poor heat dissipation, we observe additional increases in r due to laser heating, and the relative magnitudes of the measured temperature rises on different substrates scale as expected based on the optical and thermal properties of the metal films. In our measurements, the samples were surrounded by air at atmospheric pressure and room temperature. We expect that the metal surface effects we observe should generalize to other surrounding media, although corresponding changes to the heat dissipation pathways can alter the magnitude of any laser-induced heating[38]. Together, these results demonstrate that single-UCNP ratiometric thermometry remains robust in application scenarios that require placing UCNPs on the surfaces of metal structures.

Author Contributions

Ziyang Ye: investigation, methodology, visualization, writing – original draft, writing – review and editing. Laura Signor: investigation, methodology, visualization, writing – original draft, writing – review and editing. Molly Cohan: investigation, methodology, writing – review and editing. Andrea D. Pickel: conceptualization, funding acquisition, methodology, supervision, writing – original draft, writing – review and editing.

Conflicts of Interest

There are no conflicts to declare.

Data Availability

The data supporting this article have been included as part of the ESI.

Acknowledgments

This material is based upon work supported by the National Science Foundation under Grant No. 2304570. The authors also acknowledge support from the U.S. Department of Education Graduate Assistance in Areas of National Need (GAANN) fellowship program. The authors thank Ben Carlson and Kenneth Marshall for their assistance with the reflectance and transmittance measurements.

References:

1. E. M. Purcell, *Physical Review*, 1946, **69**, 681.
2. K. H. Drexhage, H. Kuhn and F. P. Schäfer, *Berichte der Bunsengesellschaft für physikalische Chemie*, 1968, **72**, 329-329.

3. K. Aslan, I. Gryczynski, J. Malicka, E. Matveeva, J. R. Lakowicz and C. D. Geddes, *Current Opinion in Biotechnology*, 2005, **16**, 55-62.
4. T. Ming, H. Chen, R. Jiang, Q. Li and J. Wang, *The Journal of Physical Chemistry Letters*, 2012, **3**, 191-202.
5. J. Enderlein, *Chemical Physics*, 1999, **247**, 1-9.
6. V.-E. Choong, Y. Park, Y. Gao, T. Wehrmeister, K. Müllen, B. R. Hsieh and C. W. Tang, *Journal of Vacuum Science & Technology A*, 1997, **15**, 1745-1749.
7. P. Anger, P. Bharadwaj and L. Novotny, *Physical Review Letters*, 2006, **96**, 113002.
8. Y. Liu, J. Zhou, S. Wen, F. Wang, H. Wu, Q. Chen, C. Zuo and D. Jin, *Nano Letters*, 2023, **23**, 5514-5519.
9. X. Yang, H. Xie, E. Alonas, Y. Liu, X. Chen, P. J. Santangelo, Q. Ren, P. Xi and D. Jin, *Light: Science & Applications*, 2016, **5**, e16134.
10. E. L. Moal, E. Fort, S. Lévêque-Fort, F. P. Cordelières, M. P. Fontaine-Aupart and C. Ricolleau, *Biophysical Journal*, 2007, **92**, 2150-2161.
11. D. Lu, S. K. Cho, S. Ahn, L. Brun, C. J. Summers and W. Park, *ACS Nano*, 2014, **8**, 7780-7792.
12. A. Rafiei Miandashti, M. E. Kordesch and H. H. Richardson, *ACS Photonics*, 2017, **4**, 1864-1869.
13. E. M. Mettenbrink, W. Yang and S. Wilhelm, *Advanced Photonics Research*, 2022, **3**, 2200098.
14. G. Lin and D. Jin, *ACS Sensors*, 2021, **6**, 4272-4282.
15. W. Park, D. Lu and S. Ahn, *Chemical Society Reviews*, 2015, **44**, 2940-2962.
16. D. M. Wu, A. García-Etxarri, A. Salleo and J. A. Dionne, *The Journal of Physical Chemistry Letters*, 2014, **5**, 4020-4031.
17. B. Harrington, Z. Ye, L. Signor and A. D. Pickel, *ACS Nanoscience Au*, 2024, **4**, 30-61.
18. T. P. van Swieten, T. van Omme, D. J. van den Heuvel, S. J. W. Vonk, R. G. Spruit, F. Meirer, H. H. P. Garza, B. M. Weckhuysen, A. Meijerink, F. T. Rabouw and R. G. Geitenbeek, *ACS Applied Nano Materials*, 2021, **4**, 4208-4215.
19. S. J. W. Vonk, T. P. van Swieten, A. Cocina and F. T. Rabouw, *Nano Letters*, 2023, **23**, 6560-6566.
20. N. Stopikowska, P. Woźny, M. Suta, T. Zheng, S. Lis and M. Runowski, *Journal of Materials Chemistry C*, 2023, **11**, 9620-9627.
21. Y. S. Touloukian, R. W. Powell, C. Y. Ho and P. G. Klemens, *Thermophysical Properties of Matter - The TPRC Data Series. Volume 1. Thermal Conductivity - Metallic Elements and Alloys*, 1971.
22. G. Chen and P. Hui, *Applied Physics Letters*, 1999, **74**, 2942-2944.
23. S. Ryu, W. Juhng and Y. Kim, *Journal of Nanoscience and Nanotechnology*, 2010, **10**, 3406-3411.
24. Y. Zeng, L. a. Li, S. Wang, F. Sun, Z. Wang, X. Tu and C. Li, *International Journal of Heat and Mass Transfer*, 2024, **227**, 125542.
25. K. L. Zhang, S. K. Chou and S. S. Ang, *International Journal of Thermal Sciences*, 2007, **46**, 580-588.
26. L.-D. Zhu, F.-Y. Sun, J. Zhu, D.-W. Tang, Y.-H. Li and C.-H. Guo, *Chinese Physics Letters*, 2012, **29**, 066301.

27. D. J. Gargas, E. M. Chan, A. D. Ostrowski, S. Aloni, M. V. P. Altoe, E. S. Barnard, B. Sanii, J. J. Urban, D. J. Milliron, B. E. Cohen and P. J. Schuck, *Nature Nanotechnology*, 2014, **9**, 300-305.
28. J. L. Braun, C. J. Szwejkowski, A. Giri and P. E. Hopkins, *Journal of Heat Transfer*, 2018, **140**, 052801.
29. A. D. Pickel and C. Dames, *Journal of Applied Physics*, 2020, **128**, 045103.
30. Q.-C. Sun, H. Mundoor, J. C. Ribot, V. Singh, I. I. Smalyukh and P. Nagpal, *Nano Letters*, 2014, **14**, 101-106.
31. L. M. Wiesholler, C. Genslein, A. Schroter and T. Hirsch, *Analytical Chemistry*, 2018, **90**, 14247-14254.
32. J. Xu, Z. Dong, M. Asbahi, Y. Wu, H. Wang, L. Liang, R. J. H. Ng, H. Liu, R. A. L. Vallée, J. K. W. Yang and X. Liu, *Nano Letters*, 2021, **21**, 3044-3051.
33. A. Teitelboim, B. Tian, D. J. Garfield, A. Fernandez-Bravo, A. C. Gotlin, P. J. Schuck, B. E. Cohen and E. M. Chan, *The Journal of Physical Chemistry C*, 2019, **123**, 2678-2689.
34. A. D. Pickel, A. Teitelboim, E. M. Chan, N. J. Borys, P. J. Schuck and C. Dames, *Nature Communications*, 2018, **9**, 4907.
35. L. H. Fischer, G. S. Harms and O. S. Wolfbeis, *Angewandte Chemie International Edition*, 2011, **50**, 4546-4551.
36. A. Sedlmeier, D. E. Achatz, L. H. Fischer, H. H. Gorris and O. S. Wolfbeis, *Nanoscale*, 2012, **4**, 7090-7096.
37. M. D. Shinn, W. A. Sibley, M. G. Drexhage and R. N. Brown, *Physical Review B*, 1983, **27**, 6635-6648.
38. C. Hernández-Álvarez, G. Brito-Santos, I. R. Martín, J. Sanchiz, K. Saidi, K. Soler-Carracedo, Ł. Marciniak and M. Runowski, *Journal of Materials Chemistry C*, 2023, **11**, 10221-10229.

The data supporting this article have been included as part of the Supplementary Information.